RSC Advances

ROYAL SOCIETY OF CHEMISTRY

www.rsc.org/advances

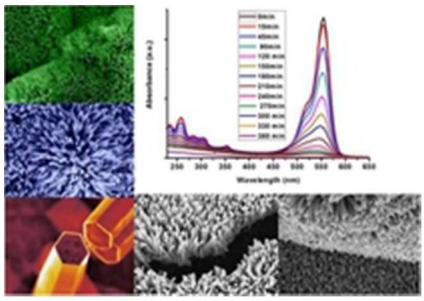

Graphical abstract
8x6mm (600 x 600 DPI)

Cite this: DOI: 10.1039/c0xx00000x

www.rsc.org/xxxxxx

ARTICLE TYPE

Superhydrophobic Polymethylsilisesquoxane pinned one dimensional ZnO nanostructures for water remediation through photo-catalysis

Ankur Gupta[1], Kunal Mondal[2], Ashutosh Sharma[2], Shantanu Bhattacharya[1,#]

ZnO nanostructures have been heavily explored for a variety of sensing properties and of late a major emphasis of researchers is to find out applications of the ZnO material in the domain of photocatalysis. ZnO nanoparticles have been found as a better alternative to other materials for removing organic dyes from pollutant water and abolition of several hazardous material etc. In this work we have developed ultra-dense high aspect ratio ZnO nano-forest like structures and explored their potential as photo-catalysts. The films formulated are super-hydrophobic (contact angle ~ 154°) in nature and have been evaluated to contain a high density of oxygen defects in the crystalline state of ZnO material (as validated through photoluminescence measurements). The samples are found to possess enhanced photo catalytic properties as measured through a dye degradation process using an UV-Vis spectrophotometer. This photo-catalytic property may be owing to the high state of defect density and also enhanced area of the interactive surface as one goes from nano-particle to nano-rod like structures. The paper gives an insight into the highly unique carpeted nanowire bundles of ZnO and offers immense utility to the realization of high efficiency remediation filters.

Introduction

From the past several decades a lot of exploration has been made for waste water treatment and abolition of several pollutants like Organic and Inorganic wastes and effluents etc. In line with this, there has been immense scope to explore nano-materials for the purpose of purification and disinfection of water and air. Due to a large enhancement of surface area provided by these materials, their role as a catalyst to accelerate remediation processes is of significant importance. Various materials (TiO_2, ZnO etc.) have been widely explored for better performance by structuring these materials into various different shapes and sizes at the meso-scopic scales. ZnO has been investigated successfully as an alternative to conventional treatment for removal of pollutant dyes from waste water. It is a low cost high band gap material and is absorbent of radiation in the UV region absorbing more light quanta than even TiO_2 [1-4]. When a source of UV light falls on ZnO the material behaves as a semiconductor producing electron/hole pairs thus increasing the overall conductivity of the material. The electron/hole pairs generated induce a complex series of reaction leading to complete degradation of dye pollutants absorbed on the surface of this material. The degradation rate is highly enhanced if the ZnO material is nano-structured as one dimensional rod like orientation of such material leads to the easy release of electrons in the gap between the rods where the dye pollutant is present. Further, ZnO nanostructures offer a very high interfacial area to the fluid that is in direct contact with the nanostructures for remediation purposes. ZnO has been found to degrade most kinds of persistent organic pollutants, such as detergents, dyes, pesticides and volatile organic compounds, under UV irradiation[5-9]. Among various factors such as aspect ratio, doping elements etc., the surface defects introduced in ZnO nanostructures play a critical role in enhancing the photocatalytic performance of the material. Defects on ZnO nanostructures have been extensively investigated by many researchers and they have been found to play a major role in offering high density adsorption sites and also offer enhanced surface reactivity. Zheng et al. showed that the oxygen vacancies and interstitial oxygen induced by solvothermal fabrication processes had a major impact on the photocatalytic activity of ZnO[7]. Wang et al. demonstrated the enhancement of photo-catalytic activity of ZnO while exposed to visible spectrum by narrowing the band gap through induced defects[8]. Li et al reported that tuning the relative concentration ratio of bulk defects to surface defects in TiO_2 nanocrystals could enhance the separation of photo-generated electro-hole pair thus improving the overall photocatalytic efficiency of this material[9]. ZnO has larger ability to absorb a fraction of the solar spectrum (because of its band width of 3.2eV) vis-à-vis TiO_2 although its photocatalytic reaction mechanism is similar to TiO_2[10,11,12], Out of variegated structures developed viz., nano belts, nano wires, nano cages, nano combs, nano springs, nano rings,[47-51] etc., One-dimensional ZnO nanostructures such as nanorods and nanowires have been investigated extensively due to the higher surface area and their superior electrochemical properties, which are attributed to dimensional anisotropy. Therefore, greater number of electrons$^-$ and protons exist on the active sites of the nano structured surface, resulting in higher activity as compared with other lower surface area nanoparticles. Although the vertical growth and associated surface area enhancement has been explored in respect of ZnO nanowires/ rods by a lot of researchers[13-18]. Very few attempts have been made that can fabricate and explore high aspect ratio vertically standing variable height nanostructures pinned to a highly nano-porous carpet. These structures would enhance the surface area multi-folds

thereby creating additional sites for binding onto dyes and chemicals so as to reduce these into harmless products and perform remediation.

In an earlier work[17], we have reported a distinct way of fabricating ZnO nano-forests having very high surface roughness and have explored their sensitivity towards detection of trace gases. In this module, we explore their application in photocatalysis at much lower power UV source (10W) making the material highly suitable to be coated in filter membranes so that remediation can be performed through membranes. The tall standing nanostructures are further annealed and a comparative study is made between annealed and unannealed samples in respect of their photo-catalytic properties using Rhodamine AR dye. We have also tried to formulate a detailed understanding of the crystal defects within these structures which leads to an enhancement in the photocatalytic properties of these structures.

Material and method

Silicon (100) p-type substrates (Source: Logistic inc. NY) were taken and thoroughly cleaned using AMD (acetone, methanol, de-ionized water). 40% hydrofluoric acid (Source: SDFCL, India) mixed in a 1:10 ratio with de-ionized water was used to passivate the silicon surface resulting in a hydrophobic surface (Contact angle ~90°). The photo-degradation of the dye Rhodamine AR (M.W. 479.02, purchased from Thomas Baker) was studied to evaluate the efficacy of the Zinc Oxide nanostructures in our experiments. Zinc nitrate [$Zn(NO_3)_2.6H_2O$] (source: Merck Specialties Pvt Ltd) and hexamethylenetetramine [$C_6H_6N_4$] (source: Merck Specialties Pvt Ltd) were utilized for the growth of ZnO one dimensional rod like structures over catalyst nanoseeds of Zinc Oxide (ZnO) implanted in a porous bed of silica. The structural characterization was performed with FESEM (Zeiss Supra 40V, Germany) and the morphology of the films with one dimensional nanostructures growing out at different heights was carried out. Further characterization of the nanostructures using X-ray diffraction (XRD) (X'Pert PRO, PAN analytical, Netherlands X-ray system) with Cu-Kα source radiation (having wavelength 1.54°A) for visualizing the vertical growth along c-axis and also measurement of the built in stresses offered by the nano-template and a correlation to the oxygen defects using photoluminescence (Xenon Lamp Spectrofluorometer (Jobin Yvon, Fluorolog-3) is carried out on these structures. We have also performed Raman characterization (by Wi Tec, Germany [Raman parameters: Objective lens =20x, Laser wavelength = 532 nm, power = 12mW, spot size = 500 nm]) for analysis of samples and UV-vis spectrophotometer (50 Bio Varian Cary spectrophotometer) to monitor the photocatalytic degradation of Rhodamine AR in the presence of these ZnO carpets. Catalytic activity is demonstrated in HPLC grade water purchased from Merck Pvt. Ltd, India. Annealing of the ZnO films was carried out at a heating rate of 10°C min^{-1} in the presence of oxygen for 1 hour. The flow rate of oxygen was set to 300 sccm.

To fabricate dense ZnO nano structures, Firstly, PMSSQ nanoparticles and PPG is all dissolved together with the nanoseeds formulated in a homogenous dispersion using PGMEA (solvent) in the following manner. PGMEA is mixed separately with PMSSQ (in 5:1 ratio by weight) by ultrasonication. Further, PPG is mixed with PGMEA with the help of vortex shaker and ultrasonicator untill proper mixing is ensured. 1g of the resulting (PMSSQ-PGMEA) solution was mixed with 5 g of (PPG-PGMEA) solution and again ultrasonicated for homogenous dispersion. This solution for convenience is named as "solution-1" In another solution, PGMEA is mixed with ZnO nanoseeds with the help of vortex shaker. This solution is named as "solution-2". ZnO nano seeds are prepared with the help of Zinc chloride (MERCK Specialties pvt ltd) (0.1M in 20 ml methanol) and NaOH pellet (SAMIR TECH-CHEM pvt ltd, India) (1.25M) which is properly mixed while stirring. The solution is mixed properly until the milky white colour appears. A drop wise solution through a syringe (with attached 0.45µm sieve) is poured onto the silicon substrate till uniform deposition of the precursor is observed. Upon heating this substrate at 200°C for 20 minutes, crystallites decompose to form ZnO particles. The above process is repeated several times to ensure uniform seed layer on the substrate surface. The layer deposited is then scrapped off the silicon surface using a sharp razor edge and collected in powder form in a vial. After accumulating sufficient weight of this powder their nano-templating is performed. Another silicon wafer (100) was cleaned using AMD protocol and hydrogen passivated by immersing it in (1:10) HF: DI water solution for ~10 seconds. Now, equal amount of solution 1 and 2 is taken and mixed properly. The solution prepared is poured drop by drop throughout the substrate with the help of syringe (5 ml) (attached with 0.45 micron sieve) until whole area of substrate is covered with the film and the film obtained was ramped up to 450°C in a hotplate and held at this temperature for 5 minutes. The film was thus heated above the decomposition temperature of PPG (>200°C) caused the evaporation of PPG and entropic disturbances in the dispersed nanoparticles (both PMMSQ and ZnO) leading to random collisions between them and eventually result in particle–particle cross linking. ZnO nanoparticles are entrapped within the PMSSQ matrix and dispersed heterogeneously through the substrate at various height of the PMSSQ film. These highly seeded matrix is used as a template to promote growth of Zinc Oxide one dimensional nano-structures in a gravity fed convection oven (set at 90° C) for over 24 hours by holding the matrix upside down over a solution of (.01M) zinc nitrate ($Zn(NO_3)_2$ and (.05M) Hexa Methylene Tetra Amine (HMTA) in DI water. The chemical reaction which occurs inside the solution initiates with a hydrolysis of HMTA in water releasing formaldehyde (HCHO) and ammonia (NH_3). of the ammonia (NH_3) slowly releases and assists in formation of Hydroxyl ions (OH^-) which leads to the minimization of bulk nucleation of Zn^{2+} in the solution. The net process output is the formulation of Zn (OH) $_2$ which dehydrates to form ZnO[17-18]. The chemical steps involved are very lucidly illustrated in equations 1~7.

$$Zn(NO_3)_2.6H_2O \rightarrow Zn^{+2} + NO_3^- \quad (1)$$

$$Zn^{+2} + 4OH^- \rightarrow Zn(OH)_4^{-2} \quad (2)$$

$$Zn^{+2} + 4NH_3 \rightarrow Zn(NH_3)_4^{+2} \quad (3)$$

$$(CH_2)_6N_4 + 6H_2O \rightarrow 4NH_3 + 6HCHC \quad (4)$$

$$(CH_2)_6N_4 + 4H_2O \rightarrow (CH_2)_6(NH)_4 + 4OH^- \quad (5)$$

$$Zn(OH)_4^{-2} \rightarrow ZnO + H_2O + 2OH^- \quad (6)$$

$$Zn(NH_3)_4^{+2} + 2OH^- \rightarrow ZnO + 4NH_3 + H_2O \quad (7)$$

The Field Emission Scanning electron microscopy (FESEM) shows highly dense vertical nanostructures grown out of nanoporous matrices. Reason for the vertical growth of ZnO nanostructures has been explained earlier by Tasker et. al. (1979)[22] in which he has described three different surface topologies of ZnO out of which the type {III} surface which resembles the present case. Since ZnO exists in wurtzite crystal form which has hexagonal unit cells having six non polar faces capped by polar oxygen and Zn atoms in basal planes. These polar faces are highly unstable and contain very high surface energy and can be defined as Tasker (III) surfaces. The tall structure growth is initiated in order to minimize the overall system energy thus becoming stable wherein the growth takes place mostly in the vertical direction. The as grown film in this work was characterized with XRD which confirmed the vertical growth of the ZnO nanostructure. Figure 5 [XRD data] showed a large peak in (002) plane signifying higher density in the vertical orientation. The optical characterization was also performed with UV Visible spectra in order to evaluate the band gap of the Zinc Oxide structures. Photoluminescence spectra suggests the presence of a differential in crystal defects owing to which the varied photocatalytic rates are observed as one uses different structures of ZnO with and without annealing.

To study the photocatalytic behaviour firstly 50-ml Rhodamine AR dye in aqueous solution (Conc.= 2×10^{-5} mol/l,) is poured in a glass petri dish after thorough mixing. The ZnO film is then held inside this solution which is top irradiated with a 10 Watts power UV lamp emitting at 254-nm wavelength. The exposure interval of this dye is varied and each sample is repeatedly characterized with UV-Visible spectrophotometer after exposing the solution for different durations. The characterization is performed by aliquoting out a 2ml solution in a quartz cuvette and then resuspending this aliquot solution after performing the UV-Visible spectrophotometer back into the source solution to maintain the pH during the whole experiment at 10. The absorbance of the Rh AR dye is measured giving absorbance peak at 554 nm.

Results and discussion:

Morphological Evaluation of the films (FESEM and TEM):

Figure 1 shows some representative FESEM images (FESEM , Quanta 200, Zeiss, Germany) taken at different zones and various magnifications of the vertically growing zinc oxide one-dimensional structures pinned in nanostructured carpets. To visualize the length of the one dimensional wire/rod-like structures, the SEM stage is inclined at 45 degree and lengthwise images of the wires are captured. The wires vary in lengths ranging from 1~5 microns. Top view of the ZnO nanowires shows the hexagonal crystal growth. (Which confirms the presence of wurtzite crystal lattice of ZnO). Sides of the hexagonal cross-section range from ~80- 150 nm. There are no morphological changes in the dimensions of annealed and un-annealed samples although there is a significant variation registered in the UV-Vis (Figure 4), XRD (Figure 5) and Photoluminescence (Figure 6) characterization of the annealed and unannealed samples.

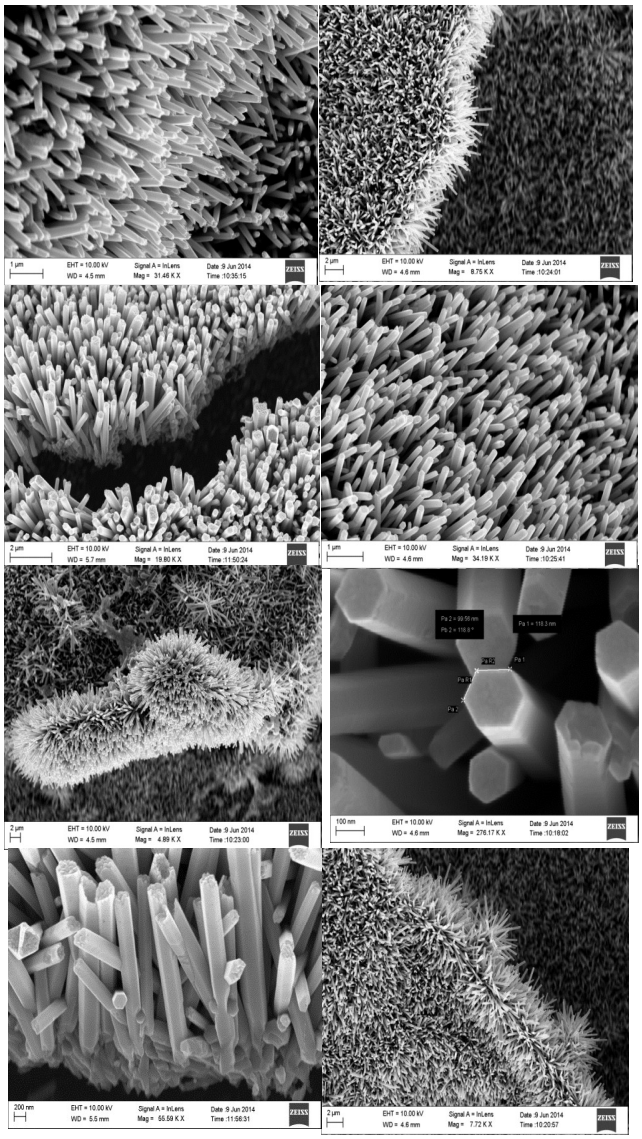

Fig.1 : FESEM images of ZnO nano-forest at various locations and in different magnifications using normal/ angled sample stage.

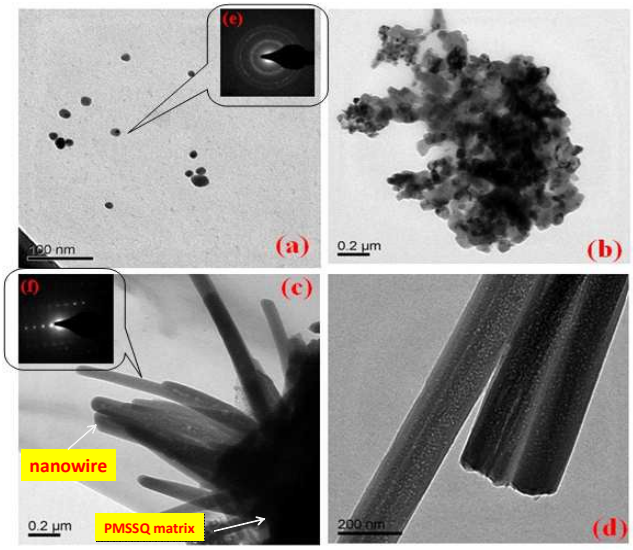

Fig. 2:(a) and (b) shows the TEM images for ZnO nanoparticles. (c) and (d) are the nanoforest scratched from the film (e) and (f) are SAED patterns of nano particles and nanoforest respectively.

Elemental mapping:

In this section we characterize the films thoroughly for elemental mapping and analysis related to structural defects. Elemental mapping and composition are studied with the help of energy dispersive X-ray spectra analyzer (Oxford instruments) [Figure 3(a)] indicate the strong presence of Zn and O elements indicating a full coverage of the pinning carpet indicating entanglement and contact between the various vertical structures as one would normally envision when they grow at high density along vertical direction. Figure 3(d) and (e) indicate the elemental presence of oxygen and zinc species in film cross-sections as indicated by green and red dots respectively.

Fig. 3: (a) shows the elemental peaks corresponding to each

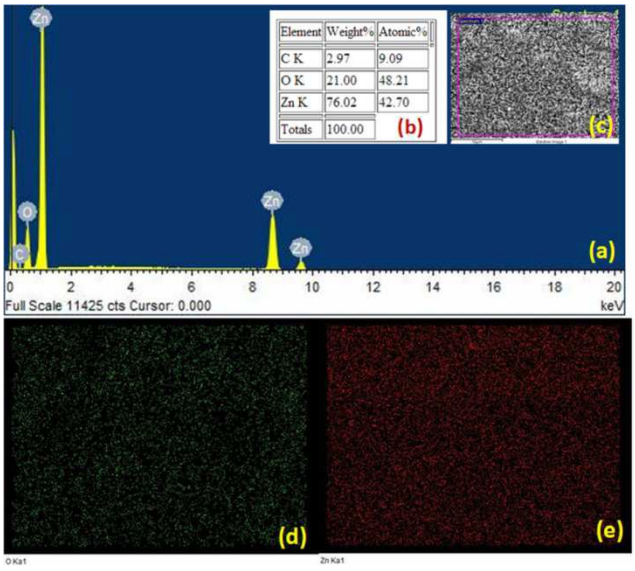

elements present over the film. (b) shows the percentage of the elements over the film (c) shows the selected region for identifying the elemental presence (d) and (e) are the elemental mapping showing the dispersion of the O and Zn particles respectively over the film

Structural analysis of the films:

UV-Visible Spectrometry:

We have performed UV-Visible spectrometry for both un-annealed and annealed samples and found a distinct change in the band gap of all samples. We hypothesize that the change in band gap in this case is purely due to a substantial change in the density of defect states. In our opinion the defect states get significantly re-distributed uniformly due to annealing of the samples. Band gap analysis is performed through Tauc plot[31] According to which the optical band gap 'E_g ' and the photon energy is 'hν' and the molar absorptivity at frequency 'ν' is provided by equation (8) where D is a constant and n is an integer

$$\alpha h\nu = D\,(h\nu - E_g)^n \qquad (8)$$

From the UV Visible spectra, we have found that annealed samples posses a red -shift of the band gap which can be seen in the figure 4. The inset shows a plot between the photon energy and the molar absorbity. The band gap goes on decreasing as we anneal the film at higher temperature. (From ~3.02eV for unannealed sample to ~2.90eV for the sample annealed at 300°C and ~2.85 eV for the sample annealed at 500°C). The photocatalytic activity as reported later is found to be the highest in the annealed sample at 500°C as annealing ensures a distribution of the defects throughout the surface of the nano-structures and a lesser band gap formulated at 500°C demonstrates an easier electron hole release.

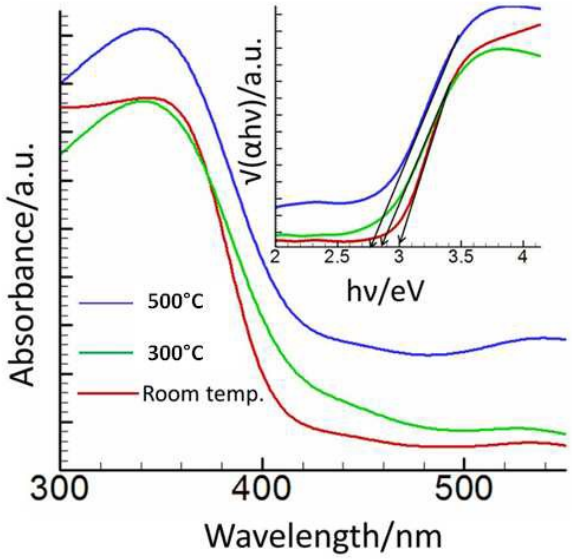

Fig. 4 shows the UV- Visible spectra of the all the samples. Inset shows the Tauc plot for determining the band gap of annealed and unannealed samples.

XRD analysis:

We have recorded the photoluminescence spectra (separately reported later in this manuscript) from which it is observed that there is an abundance of intrinsic defects within the ZnO crystal

lattice. Crystallinity is a significant parameter that determines the photocatalytic activity of a catalyst. Previous researchers viz., Eufinger et al.[20] and Yubuta et al.[21] claimed that photocatalytic activity increased with increased crystallinity in semiconductor metal oxides. Li et al.[24] concluded that the photocatalytic activity of various ZnO powders occurred mainly due to crystallinity rather than a surface area. This group was however unable to predict a specific relationship between photocatalytic activity, crystallinity and surface area.

Figure 5 shows the XRD data for all samples in which all the peaks could be safely indexed as ZnO wurtzite structure as found in the standard reference data (JCPDS: 36 1451). Crystal size can be determined for these structures and so can be the deviation from crystallinity through a Line broadening analysis. The growth of ZnO nanostructures in our case is performed through a nanocarpet entrapment process and hypothetically we can probably predict a highly pre-strained lattice structure from our method of fabrication of these structures. So, the most crucial parameter for our analysis is strain induced line broadening and XRD of the nanostructured samples should be demonstrative of lattice induced strains. Lattice strains in crystals generally manifest in two forms uniform or non-uniform strains. It has been reported that the uniformly introduced strains only causes peak shift in the XRD whereas the non-uniform strain is found to have a peak broadening. The causes of non-uniform strain can be many for example point defects, poor crystallinity etc. is no peak shift observed in samples confirming the presence of only non uniform lattice strains. We have calculated the lattice size of the ZnO crystals by Debye-Scherer's method [supplementary information S1][52,53].

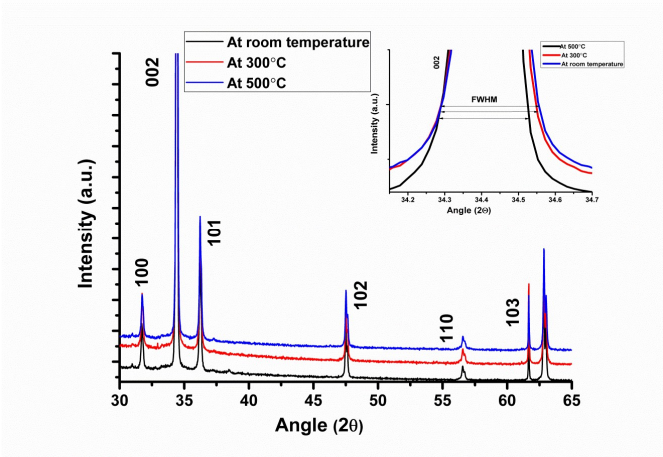

Fig. 5 shows the XRD data for un-annealed and annealed samples. Inset graph shows the difference in the peak width of un-annealed and annealed samples.

Average crystalline size of the ZnO film is 15.35 nm. Annealed samples at 300°C has crystalline size of 20.64 nm and that of 500°C has 25.32 nm which implies the sharpening of peak width thereby confirming that the crystallinity of the ZnO film is improved as the annealing temperature increases. Therefore, the annealed samples definitely posses low strains. In any event the de-straining of a lattice would always lead to a better crystallinity of the samples. The lattice strains are further predicted by Williamson hall's method [See supplementary information equation S2- S5]. The predictions of the lattice strain through this method are summarized in Table 1 along with the Lattice size. Generally, on annealing it is observed that there is an overall relaxation of the pre-strained lattice. In figure 5, inset graph shows comparison of XRD data of un-annealed and annealed samples observing the difference in peak broadening in the samples.

Table 1: Predicted crystal sizes and lattice strain values (Calculation details reported in supplementary information).

	Un-annealed	Annealed at 300°C	Annealed at 500°C
Crystalline size (nm)	15.35 +- 5.44	20.64 +-.265	25+- 5.44
Lattice strain	0.00+-0.430	0.258	0.170 +- 0.014

Photoluminescence spectra:

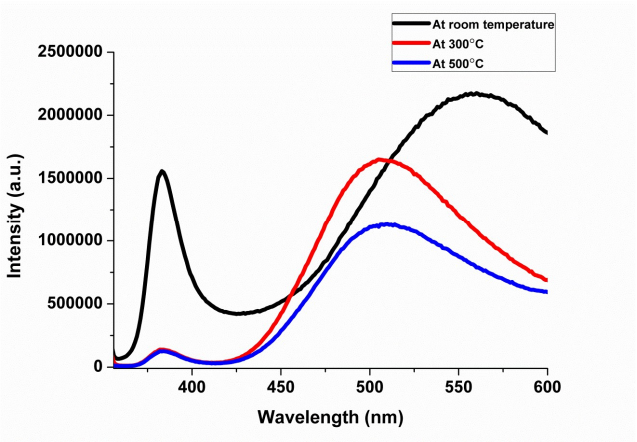

Fig. 6 shows the pl spectra of un-annealed sample, annealed at 500 and 700°C samples.

The ZnO nanostructures pinned on a silica carpet are provided with an excitation wavelength of 330 nm (3.76eV). The un-annealed film shows one huge peak at ~380nm and second peak at ~558 nm. Peak at ~380 nm is due to strong near band edge UV emission. This UV emission is attributed to the direct recombination of excitons via exciton - exciton collision process. Second peak is attributed to broad green band which is obtained from the radial recombination of photo generated hole with e^- belonging to single ionized oxygen vacancy (Vo^+) present on the surface and is observed when ZnO is fabricated under oxygen deficient condition.[17] The possibility of any other impurity in the film is very less which would have otherwise caused the green emission as in the present case as also confirmed by EDAX measurements earlier. As shown in Figure 6, the UV emission of ZnO nanostructures increases when the sample is annealed to 500˚C. This effect can be attributed to the desorption of surface adsorbed water and hydroxyl groups at high temperatures which

are unavoidable defects in such solution growth methodologies. On annealing ZnO nanowires at 500˚C in air we have observed the UV-emission to decrease substantially. The visible emission however shows overall increase due to surface defects in the ZnO nanostructures. Also there is an observable blue shift in the annealed sample with green emission peak shifting from 560 nm to ~520 nm on annealing, which could be due to corrections in crystal imperfections and lattice relaxations (Stokes shift).[23-26]

The most common defects associated with ZnO formed under lower temperatures (<100 ˚C) are oxygen vacancies (V_O), interstitial Zinc (Zn_i) and Zinc vacancies (V_{Zn}). We have earlier reported that there is an inversion of majority carriers over 275°C temperature and the ZnO changes from N to P type.[17] Here however the formation temperature is less than 100° C and thus the majority carrier still remains N-type at this low temperature. We have considered the possibility of having V_O, Zn_i, V_{Zn} defects in our nanostructures. Considering the energy level diagrams for ZnO crystals[30] [Supplementary Figure S1] and the observation from the PL spectra of all the visible emission due to defects falling in the green region (with the energy interval of 2.24 – 2.46 eV), there are two possibilities for this to occur. First is the transition from conductance band to V_{Zn} which is located at ~ 0.8 eV above the valence band, hence resulting in a emission of ~ 2.5 eV which is somewhat close to the observations made in our case. Second is due to hole capture by V_O^o which occurs in three states (uncharged, singly charged and doubly charged) and occupy the energy levels from ~2.17-2.5 eV above the valence band. The presence of Zinc interstitial Zn_i can be ruled out because firstly the formation energy of Zn_i is quite large as compared to other defects and if Zn_i would have really existed we would have observed a transition from Zn_i to the top of valence band with emission energy corresponding to ~2.8 eV but no such emission has been observed in the spectra rule out one of the other two possibilities we observe the results from annealing of ZnO nanowires in oxygen atmosphere. Annealing was carried out with heating rate of 10˚C/min and annealing time of 1 hour, the cooling was performed using furnace cooling. The flow rate of oxygen used in the annealing was set to 300 sccm. To understand the defect formation in the crystal lattice, defect formation at higher temperatures can be written as:

$$ZnO = Zn_{Zn}(V_{Zn}^x)O_O(V_O^x) \quad (9)$$

The concentration of the vacancies formed can be estimated as

$$[V_O^x] = e^{\left(-\frac{\varepsilon_O}{kT}\right)} \quad (10)$$

$$[V_{Zn}^x] = e^{\left(-\frac{\varepsilon_{Zn}}{kT}\right)} \quad (11)$$

Where ε_o and ε_{Zn} are formation energies of V_O^x and V_{Zn}^x respectively (Schottky defect), k is the Boltzmann constant and T is thermodynamic temperature, which was considered, approximately, as annealing temperature. The dependence of partial pressure due to O_2 (p_{O_2}) could be summarized as in equations below.

$$\frac{1}{2}O_2 + V_O^x = O_O^x \qquad [V_O^x] \propto p_{O_2}^{-1/2} \quad (12)$$

$$\frac{1}{2}O_2 = V_{Zn}^x + O_O^x \qquad [V_{Zn}^x] \propto p_{O_2}^{1/2} \quad (13)$$

From the above equations, it can be figured out that Oxygen vacancies should decrease with the increase in p_{O_2} and Zinc vacancies should increase with increase in p_{O_2} and vice versa. Figure 7 shows the comparison with oxygen annealing at 300˚C and 500°C. In both the occasions it is observed that emission intensity decreases in the case of O_2 atmosphere i.e. an increase in p_{O_2} caused a decrease in emission intensity. Therefore we can conclude that the one of the main defects in the ZnO crystal is V_O. The oxygen vacancy can exist in three possible charged state viz. neutral V_O^x, singly ionized V_O^+ and doubly ionized V_O^{++}. The singly ionized state V_O^+ is found to be thermodynamically unstable by calculations based on first principle. However some researchers suggest that V_O^+ plays a very crucial role in the green emission of the samples. At higher temperatures (500˚C) due to local lattice relaxations conditions favourable to V_O^+ formation is achieved. A photo-generated hole absorption by a neutral oxygen vacancy under relatively low excitation results in the formation of metastable V_O^+ which emits the green wavelength. The metastable state V_O^+ would eventually after some time convert into more stable V_O^{++}[23-30]. This explains the entire room temperature PL phenomenon observed in the samples and establishes the presence of oxygen vacancies in the crystal of ZnO.

Raman characterization:

In order to understand the properties of the nanostructures, Raman characterization is further performed and observed and some peaks which may be possibly due to phonon confinement effect, local heating, stresses etc. are observed. Inclusive study of the phonons in ZnO and their temperature dependence is illustrated below on a ZnO single crystal grown by the aforementioned approach Data shown in the figure indicates an intense E2 (high) mode which confirms the perfect Wurtzite crystal structure of ZnO. Wurtzite crystal belongs to space group C_{6v} with two formula units in the primitive cell. The zone centre optical phonons can be classified according to the following representations: $T_{opt} = A_1 + E_1 + 2E_2 + 2B_1$ where, B_1 modes are silent modes, A_1 and E_1 modes are the polar modes whereas E_2 modes are non polar and Raman active only and consists of low and high frequency phonons. They are associated with vibration of oxygen atoms and Zn sub-lattice. E1 (LO) peaks are associated with several defects such as oxygen vacancies, Zn_i (Zinc interstitials)[41,43] etc. Unannealed samples has stronger peak indicating the higher presence of oxygen vacancies. Once annealing in the presence of oxygen is performed followed by another round of Raman characterization these peaks diminute confirming the reduction of oxygen vacancies ZnO crystal lattice. It is interesting to note that the E_1(LO) phonon mode in high-temperature-annealed samples has undergone line width broadening and down shift in frequency with asymmetric line shape. Although this may be due to strong coupling of free carriers with E_1 (LO) mode, the influence of change in particle size due to high temperature annealing cannot be ruled out here. Using the Gaussian–Lorenz fitting, there is a weak shoulder peak in the low frequency direction of intense vibration at 439 cm^{-1}, which correspond to the E_1 (TO) mode. Moreover, the acoustic phonon overtone and optical phonon overtone with A_1 symmetry locate at 203 and 331 cm^{-1}, respectively. As per research

reported earlier the acoustic combination of A_1 and E_2 was observed around 1101 cm^{-1}. Our result also show a broad band between 1060 and 1200 cm^{-1}, which confirms the above-mentioned report. The broad peaks at 334, 663, 1145 cm^{-1} should belong to the multi-phonons process[43-46].

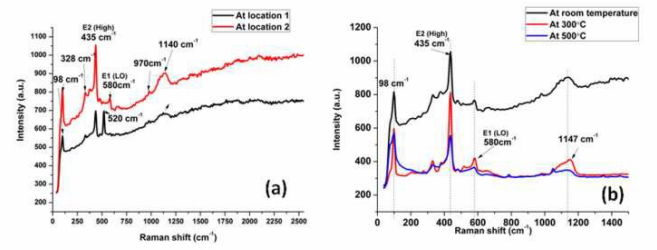

Fig. 7 shows the Raman spectra (a) for ZnO film in un-annealed condition (b) ZnO film annealed at 300 and 500°C.

Contact angle measurement:

We have also measured the contact angle to examine the nature of the film surface. These films are found to be super hydrophobic in nature probably again due to the tall standing structure of the Zinc Oxide films . Contact angle with water droplet is found to be ~154° and that of glycerol is found to be ~156°. Contact angle hysteresis is also evaluated to be ~4.2° which proves super hydrophobic nature of the film[54]. [as shown in the figure S3 of supplementary information] Super-hydrophobic films of porous silica have already demonstrated very high capacitance as reported by Bok et. al.[55] We hypothesize that this superhydrophobicity may be the reason of a high charge storage inbetween the tall nanowire structures thus enabling accelerated dye remediation as detailed later.

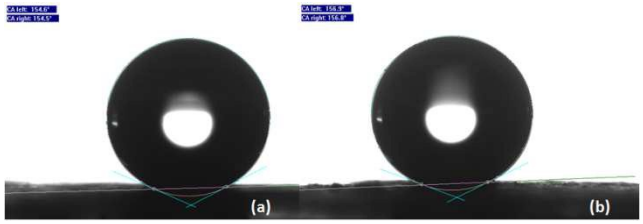

Fig. 8 shows the contact angles for the ZnO nanoforest in which figure (a) shows the Contact angle (~154°) with water drop (b) Contact angle with glycerol (~156°) with film depicting the hydrophobic nature of the film.

Photocatalytic Study:

Photocatalytic efficiency of the PMSSQ embedded ZnO films is tested for degradation of Rhodamine AR dye whose molecular formula is $C_{28}H_{31}ClN_2O_3$. The schematic of the photocatalytic mechanism undergone by the dye in the presence of ZnO one dimensional nanostructures is shown below in Figure 9. This reaction has been used as a model reaction for the evaluation of photocatalytic efficiency of various metal oxide nano particles (TiO_2, ZnO and so forth). In an aqueous photo-catalytic system, the induced hole is used to oxidise the water to a powerful oxidising radical species (the hydroxyl radical mainly) which further helps in the oxidisation of an organic/model compound. Usually, the electron produced on UV irradiation is either taken up by an electron acceptor such an oxygen molecule (O_2) or by a metal ion. If the pH is greater than a point of zero charge, a superoxide radical is formulated when it is taken up by the O_2. This further reacts with water to form hydrogen peroxide $(H_2O_2)-$ which on further oxidation generates $OH^{\cdot}$ free radical. These $OH^{\cdot}$ radicals further attack the reactant species (Dye molecule) to degrade them into carbon dioxide (CO_2), water and minerals (i.e. mineralisation). The metal ion (if any) can be reduced to its lower valence state and can be deposited on the surface of the catalyst if the induced electron is taken by a metal ion having a redox potential more than the band gap of the photo-catalyst. Because of the preferential ability of oxygen to react other competent species, oxidation of metal ions are rare Overall, the electron transfer process becomes more efficient if the reaction species are pre-adsorbed on the surface of the catalyst. In short, the induced electron-hole pair helps in the formation of hydroxyl radicals (a primary oxidant) which are ultimately used in oxidising organic and inorganic species present in the reaction system[37-39].

$$ZnO + hv \longrightarrow e^-_{CB} + h^+_{VB}$$

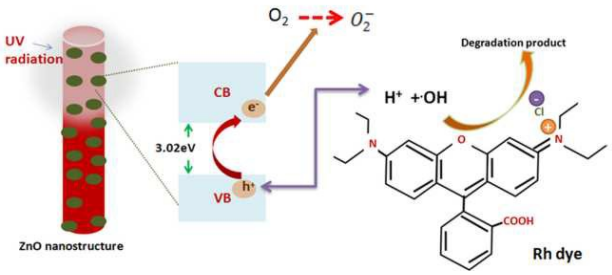

$$h^+_{VB} + H_2O \longrightarrow H^+ + {}^{\cdot}OH$$

$$e^-_{CB} + O_2 \longrightarrow O_2^{\cdot-}$$

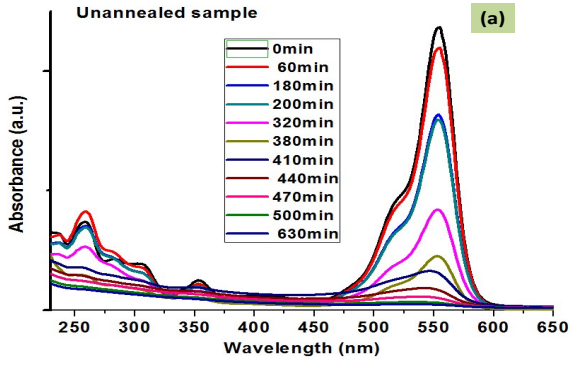

$$O_2^{\cdot-} + {}^{\cdot}OH + \text{Rh dye} \longrightarrow \text{degraded product}$$

Fig. 9 shows the schematic showing the photocatalytic phenomena.

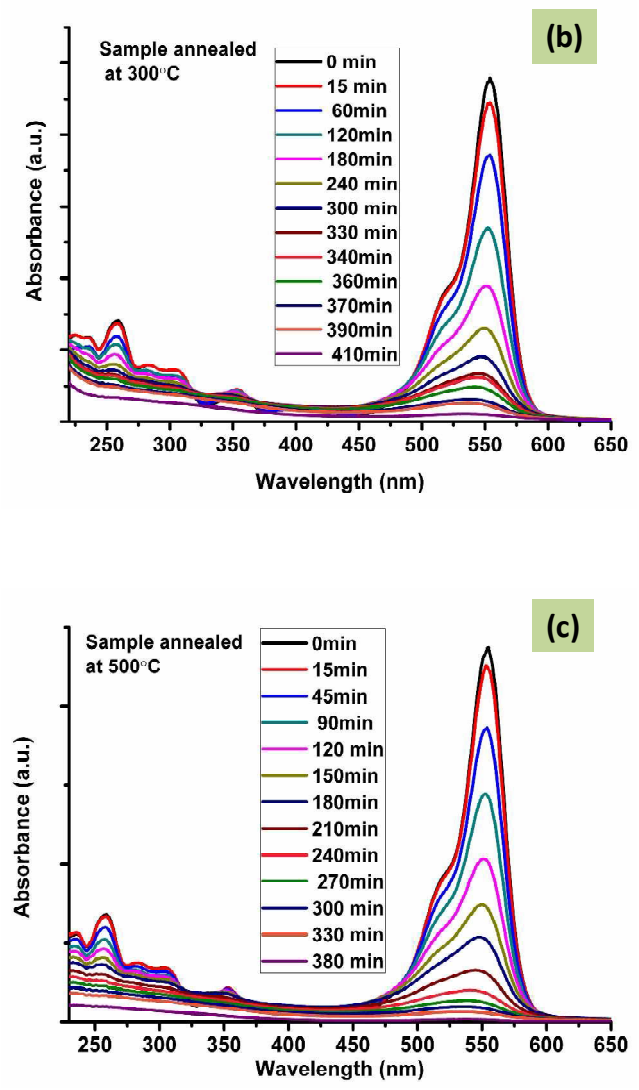

Fig. 10 shows the photo catalytic response of un-annealed (a) and annealed samples at 300°C (b) and 500°C (c) respectively.

Figure 10 shows the UV Visible spectra of the degrading dye molecule after several instants of time for all the sample unannealed and annealed at 300°C and 500°C) . Absorbance of the dye exposed to UV light is recorded upto the instant that the dye completely degrades. In supplementary information, Figure S2 shows the corresponding colour change due to dye degradation post UV exposure after various time intervals are elapsed. Figure 11 shows the degradation rate of the dye representing reaction rate of all the samples. From the behaviour of the oxygen annealed sample if is obvious that there is an enhanced reaction rate. We hypothesize that this additional treatment minimizes the release of Oxygen as it replaces atoms within the ZnO lattice thus creating more surface defects on the one dimensional nanostructures. There occurs a significant difference in Rh dye degradation rate as correlated with the different morphologies and crystallinity at both UV wavelengths. The log-scale in the inset shows linear relationship with the irradiation time, indicating that the photo-degradation process of Rh AR dye to demonstrate pseudo-first-order kinetics. As per the reaction kinetics the slope represented in the inset is representative of the reaction rate constant. The rate constant of annealed samples are found to be higher than the unannealed sample.

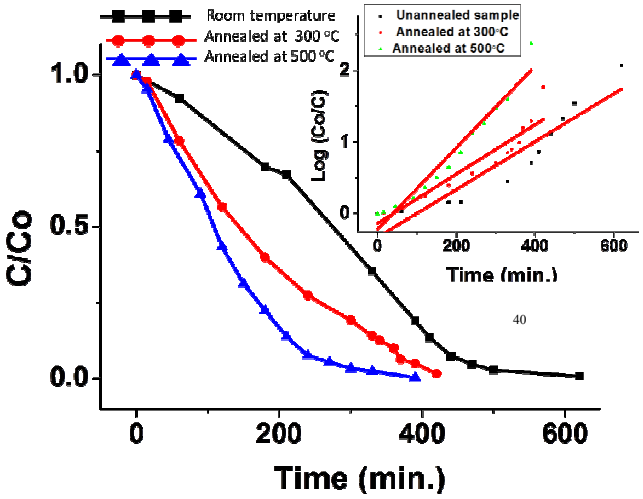

Fig. 11 shows the degradation rate of Rh dye with UV irradiation time. C_o is the initial concentration of the dye and C is the reaction concentration with time. Inset is the log plot of C_o/C with respect to time providing information on the reaction rate constant of the dye degradation process.

Reusability of photocatalyst :

We have performed the experiment to check the cyclic behaviour of the film elements in order for this to qualify for commissioning within a filter. Cycle1 has taken 380min, Cycle 2: 395min and cycle3 :(410min) and cycle4: (435min). Degradation time of the dye is plotted with number of use of dye which is shown in figure 12.

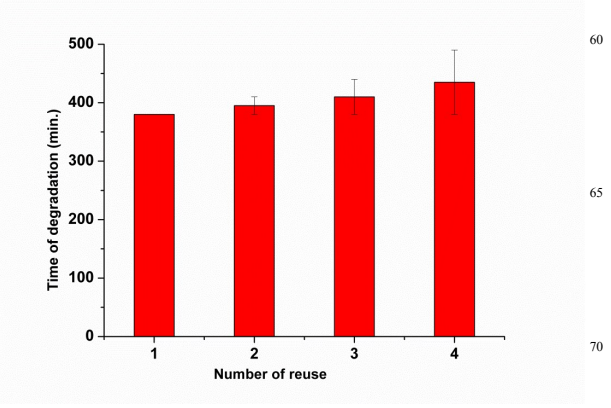

Fig. 12 shows the reusability test for the sample in which sample is tested four times and dye degradation time is measured each time.

Conclusion:

We present a distinct approach to produce ultrahigh surface area ZnO nano structures which undoubtedly can provide higher active sites for any kind of application viz., biosensing, gas

sensing, photocatalysis etc. where the analyte of interest while being in contact with the nanostructures positively affect the process of degradation. The nano-structures created has varied morphologies and we have explored the photocatalytic nature of the nano-structures using very low (10W) UV irradiation Further we have developed an overall scheme through which the nano-structures are pinned down to a carpet which allows them to be patterned as high density water remediation filters. Therefore it can be concluded that defects in one dimensional ZnO nanostructures get enhanced significantly as the structures are pinned to a surface as a carpet. Such an increase is advantageous to photo-catalytic degradation effects of these one-dimensional structures and could enhance charge separation and reduce electron-proton recombination losses and also better serve as highly dense active sites for dye degradation reaction.

Acknowledgement:

Authors gratefully acknowledge the DST Unit on Soft Nano-fabrication, at I.I.T. Kanpur for providing and the National Programme for Materials and Smart Structures (NPMASS) for providing financial support for this work.

Notes

[1]Department of Mechanical Engineering, Indian Institute of Technology Kanpur, India

[2]Department of Chemical Engineering, Indian Institute of Technology Kanpur, India

E-mail of corresponding author: bhattacs@iitk.ac.in

References

1 Lim, J. H. et al. UV Electroluminescence Emission from ZnO Light-Emitting Diodes Grown by High-Temperature Radiofrequency Sputtering. Adv. Mater. 18, 2720–2724 (2006).

2 Lansdown, A. B. G. & Taylor, A. Zinc and titanium oxides: promising UV absorbers but what influence do they have on the intact skin? Int. J. Cosmet. Sci. 19, 167–172 (1997).

3 Fujishima, Akira, Tata N. Rao, and Donald A. Tryk. "Titanium dioxide photocatalysis." Journal of Photochemistry and Photobiology C: Photochemistry Reviews 1.1 (2000): 1-21.

4 Mondal, Kunal, Jitendra Kumar, and Ashutosh Sharma. "TiO_2-nanoparticles-impregnated photocatalytic macroporous carbon films by spin coating." Nanomaterials and Energy 2.3, Themed Issue-Photocatalysis for Energy and Environment (2013): 121-133.

5 Ali, Arshid M., Emma AC Emanuelsson, and Darrell A. Patterson. "Photocatalysis with nanostructured zinc oxide thin films: The relationship between morphology and photocatalytic activity under oxygen limited and oxygen rich conditions and evidence for a Mars Van Krevelen mechanism." Applied Catalysis B: Environmental 97.1 (2010): 168-181.

6 Soltaninezhad, M., and A. Aminifar. "Study nanostructures of semiconductor zinc oxide (ZnO) as a photocatalyst for the degradation of organic pollutants." INTERNATIONAL JOURNAL OF NANO DIMENSION (IJND) (2011).

7 Zheng, Y. et al. Luminescence and Photocatalytic Activity of ZnO Nanocrystals: Correlation between Structure and Property. Inorg. Chem. 46, 6675–6682 (2007).

8 Wang, Junpeng, Zeyan Wang, Baibiao Huang, Yandong Ma, Yuanyuan Liu, Xiaoyan Qin, Xiaoyang Zhang, and Ying Dai. "Oxygen vacancy induced band-gap narrowing and enhanced visible light photocatalytic activity of ZnO." ACS applied materials & interfaces 4, no. 8 (2012): 4024-4030.

9 Lin, C.-C. & Li, Y.-Y. Synthesis of ZnO nanowires by thermal decomposition of zinc acetate dihydrate. Mater. Chem. Phys. 113, 334–337 (2009).

10 Sakthivel, S., B. Neppolian, M. V. Shankar, B. Arabindoo, M. Palanichamy, and V. Murugesan. "Solar photocatalytic degradation of azo dye: comparison of photocatalytic efficiency of ZnO and TiO 2." *Solar Energy Materials and Solar Cells* 77, no. 1 (2003): 65-82.

11 Peternel, I.T., et al., Comparative study of UV/TiO2, UV/ZnO and photo-Fenton processes for the organic reactive dye degradation in aqueous solution. Journal of Hazardous Materials, 2007. 148(1-2): p. 477-484.

12 Daneshvar, N., D. Salari, and A.R. Khataee, Photocatalytic degradation of azo dye acid red 14 in water on ZnO as an alternative catalyst to TiO_2. Journal of Photochemistry and Photobiology A: Chemistry, 2004. 162(2-3): p. 317-322.

13 Wang, H., et al., Comparison of dye degradation efficiency using ZnO powders with various size scales. Journal of Hazardous Materials, 2007. 141(3): p. 645-652.

14 Akyol, A., H.C. Yatmaz, and M. Bayramoglu, Photocatalytic decolorization of Remazol Red RR in aqueous ZnO suspensions. Applied Catalysis B: Environmental, 2004. 54(1): p. 19-24.

15 Ma, Chunyu, Zhihua Zhou, Hao Wei, Zhi Yang, Zhiming Wang, and Yafei Zhang. "Rapid large-scale preparation of ZnO nanowires for photocatalytic application." Nanoscale research letters 6, no. 1 (2011): 1-5.

16 Greene, Lori E., Matt Law, Joshua Goldberger, Franklin Kim, Justin C. Johnson, Yanfeng Zhang, Richard J. Saykally, and Peidong Yang. "Low-temperature wafer-scale production of ZnO nanowire arrays", Angewandte Chemie International Edition 42, no. 26 (2003): 3031-3034.

17 Gupta Ankur, S. S. Pandey, Monalisha Nayak, Arnab Maity, Subhashish Basu Majumder, and Shantanu Bhattacharya. "Hydrogen sensing based on nanoporous silica-embedded ultra dense ZnO nanobundles." RSC Advances 4, no. 15 (2014): 7476-7482.

18 Gupta, Ankur, Shashank S. Pandey, and Shantanu Bhattacharya. "High aspect ZnO nanostructures based hydrogen sensing." In Proceeding of International Conference On Recent Trends In Applied Physics And Material Science: RAM 2013, vol. 1536, no. 1, pp. 291-292. AIP Publishing, 2013.

19 Jang, Y.J., C. Simer, and T. Ohm, Comparison of zinc oxide nanoparticles and its nano-crystalline particles on the photocatalytic degradation of methylene blue. Materials Research Bulletin, 2006. 41(1): p. 67-77.

20 Eufinger, K., et al., Effect of microstructure and crystallinity on the photocatalytic activity of TiO2 thin films deposited by dc magnetron sputtering. Journal of Physics D: Applied Physics, 2007(17): p. 5232.

21 Yubuta, K., et al., Structural characterization of ZnO nano-chains studied by electron microscopy. Journal of Alloys and Compounds, 2007. 436(1-2): p. 396-399.

22 Tasker, P. W. "The stability of ionic crystal surfaces." Journal of Physics C: Solid State Physics 12, no. 22 (1979): 4977.

23 Erhart, Paul, Karsten Albe, and Andreas Klein. "First-

principles study of intrinsic point defects in ZnO: Role of band structure, volume relaxation, and finite-size effects." Physical Review B 73, no. 20 (2006): 205203.

24 Li, D. and H. Haneda, Morphologies of zinc oxide particles and their effects on photocatalysis. Chemosphere, 2003. 51(2): p. 129-137.

25 Gong, Yinyan, Tamar Andelman, Gertrude F. Neumark, Stephen O'Brien, and Igor L. Kuskovsky. "Origin of defect-related green emission from ZnO nanoparticles: effect of surface modification." Nanoscale Research Letters 2, no. 6 (2007): 297-302.

26 Zu, P., Z. K. Tang, George KL Wong, M. Kawasaki, A. Ohtomo, H. Koinuma, and Y. Segawa. "Ultraviolet spontaneous and stimulated emissions from ZnO microcrystallite thin films at room temperature." Solid State Communications 103, no. 8 (1997): 459-463.

27 Banerjee, D., J. Y. Lao, D. Z. Wang, J. Y. Huang, Z. F. Ren, D. Steeves, B. Kimball, and M. Sennett. "Large-quantity free-standing ZnO nanowires." Applied Physics Letters 83, no. 10 (2003): 2061-2063.

28 Lyu, Seung Chul, Ye Zhang, Hyun Ruh, Hwack-Joo Lee, Hyun-Wook Shim, Eun-Kyung Suh, and Cheol Jin Lee. "Low temperature growth and photoluminescence of well-aligned zinc oxide nanowires." Chemical Physics Letters 363, no. 1 (2002): 134-138.

29 Lin, Bixia, Zhuxi Fu, and Yunbo Jia. "Green luminescent center in undoped zinc oxide films deposited on silicon substrates." Applied Physics Letters 79, no. 7 (2001): 943-945.

30 Schmidt-Mende, Lukas, and Judith L. MacManus-Driscoll. "ZnO–nanostructures, defects, and devices." Materials today 10, no. 5 (2007): 40-48.

31 Kumar B, Gong H, Chow SY, Tripathy S, Hua Y. Photoluminescence and multiphonon resonant Raman scattering in low temperature grown ZnO nano-structures. Appl Phys Lett 2006; 89:7.

32 M. Rajalakshmi, Akhilesh K. Arora, B.S. Bendre, Shailaja Mahamuni, Optical phonon confinement in zinc oxide nanoparticles, J. Appl. Phys. 87 (2000) 2445.

33 P. Wang, G. Xu, P. Jin, Size dependence of electron-phonon coupling in ZnO nanowires, Phys. Rev. B 69 (2004) 113303.

34 H.M. Cheng, H.C. Hsu, Y.K. Tseng, L.J. Lin, W.F. Hsieh, Raman scattering and efficient UV photoluminescence from well-aligned ZnO nanowires epitaxially grown on GaN buffer layer, J. Phys. Chem. B 109 (2005) 8749

35 J.F. Scott, UV resonant Raman scattering in ZnO, Phys. Rev. B 2 (1970) 1209.

36 K.A. Alim, V.A. Fonoberov, A.A. Balandin, Origin of the optical phonon frequency shifts in ZnO quantum dots, Appl. Phys. Lett. 86 (2005) 053103.

37 Kabra, K., R. Chaudhary, and R.L. Sawhney, Treatment of hazardous organic and inorganic compounds through aqueous-phase photocatalysis: A review. Industrial and Engineering Chemistry Research, 2004. 43(24): p. 7683-7696.

38 Chen, C.-C., Degradation pathways of ethyl violet by photocatalytic reaction with ZnO dispersions. Journal of Molecular Catalysis A: Chemical, 2007. 264(1-2): p. 82-92

39 Hoffmann, M.R., et al., Environmental Applications of Semiconductor Photocatalysis. Chemical Reviews, 1995. 95(1): p. 69-96.

40 Li, Seu Yi, Pang Lin, Chia Ying Lee, and Tseung Yuen Tseng. "Field emission and photofluorescent characteristics of zinc oxide nanowires synthesized by a metal catalyzed vapor-liquid-solid process." Journal of applied physics 95, no. 7 (2004): 3711-3716.

41 Kumar B, Gong H, Chow SY, Tripathy S, Hua Y. Photoluminescence and multiphonon resonant Raman scattering in low temperature grown ZnO nano-structures. Appl Phys Lett 2006; 89:7.

42 M. Rajalakshmi, Akhilesh K. Arora, B.S. Bendre, Shailaja Mahamuni, Optical phonon confinement in zinc oxide nanoparticles, J. Appl. Phys. 87 (2000) 2445.

43 P. Wang, G. Xu, P. Jin, Size dependence of electron-phonon coupling in ZnO nanowires, Phys. Rev. B 69 (2004) 113303.

44 H.M. Cheng, H.C. Hsu, Y.K. Tseng, L.J. Lin, W.F. Hsieh, Raman scattering and efficient UV photoluminescence from well-aligned ZnO nanowires epitaxially grown on GaN buffer layer, J. Phys. Chem. B 109 (2005) 8749.

45 J.F. Scott, UV resonant Raman scattering in ZnO, Phys. Rev. B 2 (1970) 1209.

46 K.A. Alim, V.A. Fonoberov, A.A. Balandin, Origin of the optical phonon frequency shifts in ZnO quantum dots, Appl. Phys. Lett. 86 (2005) 053103.

47 He, Fa-Quan, and Ya-Pu Zhao. "Growth of ZnO nanotetrapods with hexagonal crown." Applied physics letters 88.19 (2006): 193113.

48 Cheng, Wende, Ping Wu, Xingquan Zou, and Tan Xiao. "Study on synthesis and blue emission mechanism of ZnO tetrapod like nanostructures." *Journal of applied physics* 100, no. 5 (2006): 054311.

49 He, Q.F. and Zhao Y.P., Growth and optical properties of peculiar ZnO tetrapods, J. Phys. D: Appl. Phys., 2009, 39, p. 2105–2108.

50 Huang, Shengli, Qianqian Yang, Binbin Yu, Dingguo Li, Ruisheng Zhao, Shuping Li, and Junyong Kang. "Controllable synthesis of branched ZnO/Si nanowire arrays with hierarchical structure." *Nanoscale research letters* 9, no. 1 (2014): 1-9.

51 Deng, Da, Scot T. Martin, and Shriram Ramanathan. "Synthesis and characterization of one-dimensional flat ZnO nanotower arrays as high-efficiency adsorbents for the photocatalytic remediation of water pollutants." *Nanoscale* 2, no. 12 (2010): 2685-2691.

52 Zak, A. Khorsand, WH Abd Majid, M. Ebrahimizadeh Abrishami, and Ramin Yousefi. "X-ray analysis of ZnO nanoparticles by Williamson–Hall and size–strain plot methods." *Solid State Sciences* 13, no. 1 (2011): 251-256.

53 Mote, V. D., Y. Purushotham, and B. N. Dole. "Williamson-Hall analysis in estimation of lattice strain in nanometer-sized ZnO particles." *Journal of Theoretical and Applied Physics* 6, no. 1 (2012): 1-8.

54 Kulinich, S. A., and M. Farzaneh. "Effect of contact angle hysteresis on water droplet evaporation from super-hydrophobic surfaces." *Applied Surface Science* 255, no. 7 (2009): 4056-4060.

55. Bok S., Lubguban A.A., Gao Y., Bhattacharya S., Gillis K., Gupta S., Sharp P.R. and Gangopadhyay S., "Synthesis of electrochemically active Silica matrix bound carbon based electrode materials via Sol-Gel process", *Journal of Electrochemical Society*, Vol. 155, No. 5, K91-K95, 2008.